Acta Crystallographica Section D
**Biological Crystallography**
ISSN 0907-4449

# Structure of human DSP18, a member of the dual-specificity protein tyrosine phosphatase family

**Dae Gwin Jeong,[a] Yoon Hea Cho,[a] Tae-Sung Yoon,[a] Jae Hoon Kim,[a,b] Jeong Hee Son,[a] Seong Eon Ryu[a]* and Seung Jun Kim[a]***

[a]Systemic Proteomics Research Center, Korea Research Institute of Bioscience and Biotechnology, 52 Eoeun-Dong, Yuseong-Gu, Daejeon 305-333, South Korea, and [b]Faculty of Biotechnology, College of Applied Life Science, Cheju National University, Aradong 1, Jeju 690-756, South Korea

Correspondence e-mail: ryuse@kribb.re.kr, ksj@kribb.re.kr

Received 23 November 2005
Accepted 19 March 2006

**PDB Reference:** DSP18, 2esb, r2esbsf.

The human dual-specificity protein phosphatase 18 (DSP18) gene and its protein product have recently been characterized. Like most DSPs, DSP18 displays dephosphorylating activity towards both phosphotyrosine and phosphothreonine residues. However, DSP18 is distinct from other known DSPs in terms of the existence of ~30 residues at the C-terminus of the catalytic domain and an unusual optimum activity profile at 328 K. The crystal structure of human DSP18 has been determined at 2.0 Å resolution. The catalytic domain of DSP18 adopts a fold similar to that known for other DSP structures. Although good alignments are found with other DSPs, substantial differences are also found in the regions surrounding the active site, suggesting that DSP18 constitutes a unique structure with a distinct substrate specificity. Furthermore, the residues at the C-terminus fold into two antiparallel $\beta$-strands and participate in extensive interactions with the catalytic domain, explaining the thermostability of DSP18.

## 1. Introduction

Mitogen-activated protein (MAP) kinases play an important role in controlling various cellular processes, including cell growth, differentiation, transcription and metabolism (Chang & Karin, 2001). MAP kinases (MAPKs) are fully activated through dual phosphorylation of tyrosine and threonine residues in their activation loops. Further, MAPK signalling is tightly controlled by the dephosphorylation activity of dual-specificity protein phosphatases (DSPs) that are positively inducible at the transcriptional level by MAPK activation, thus representing feedback regulation (Camps *et al.*, 2000). The human genome is estimated to encode 61 DSPs to meet the demand for distinct functions implicated in diverse cellular signalling (Alonso *et al.*, 2004). The human protein tyrosine phosphatase (PTP) family, which can dephosphorylate MAPKs, estimated to comprise 30 members, is divided into MAP kinase protein phosphatases (MKPs) and atypical DSPs according to structural and functional characteristics (Alonso *et al.*, 2004; Farooq & Zhou, 2004). 11 'typical' DSPs, also known as MAP kinase phosphatases (MKPs), have an N-terminal MAPK-binding domain in addition to the catalytic domain, while 19 atypical DSPs contain only a catalytic domain and are thus smaller enzymes than MKPs. *Vaccinia* H1-related dual-specific protein phosphatase (VHR) is the first atypical DSP which has been well characterized structurally and biologically (Yuvaniyama *et al.*, 1996; Alonso *et al.*, 2001). However, many atypical DSPs are still poorly characterized and their functions unrelated to those of MAPKs remain to be elucidated.

DSP18 is a member of the atypical DSP family and has recently been cloned and characterized (Wu *et al.*, 2003).

**Table 1**
Data-collection and refinement statistics.

Values in parentheses are for the highest resolution bin.

| | |
|---|---|
| Data collection | |
| Space group | $C222_1$ |
| Unit-cell parameters (Å, °) | $a$ = 35.74, $b$ = 96.08, $c$ = 116.65, $\alpha = \beta = \gamma = 90$ |
| Resolution (Å) | 2.0 |
| Unique reflections | 13507 |
| Total reflections | 58984 |
| Completeness (%) | 96.2 (93.6) |
| $R_{\rm merge}$† (%) | 10.7 (19.6) |
| $I/\sigma(I)$ | 13.4 (8.1) |
| Refinement | |
| No. of reflections | 13478 |
| Total No. of atoms | 1459 |
| No. of protein atoms | 1271 |
| No. of non-protein atoms | 188 |
| $R_{\rm cryst}/R_{\rm free}$ | 15.9/18.9 |
| R.m.s. deviations | |
| Bond distances (Å) | 0.008 |
| Bond angles (°) | 1.4 |
| Impropers (°) | 0.8 |
| Dihedrals (°) | 22.7 |
| Temperature factors | |
| Protein (Å$^2$) | 19.2 |
| Hetero atoms (Å$^2$) | 34.7 |
| Solvent atoms (Å$^2$) | 33.9 |

† $R_{\rm merge} = \sum_i |I_i - \langle I\rangle| / \sum |\langle I\rangle|$, where $I$ is the intensity of the $i$th meaasurement of an equivalent reflection with indices *hkl*.

DSP18 is an active phosphatase *in vitro* and is widely expressed in various tissues. In terms of substrate specificity, the catalytic activity of DSP18 shows a preference for phosphotyrosine (pTyr) over phosphothreonine (pThr) substrates. Notably, DSP18 displays unusual activity profiles. The optimum temperature for DSP18 activity is 328 K and 80% of the optimum activity is retained up to 343 K (Wu *et al.*, 2003). The DSP18 gene encodes 188 residues including a DSP motif and an additional flanking 30 residues at the C-terminus. However, the biological implications regarding thermostability and the function of the C-terminal (CT) motif are still not known. Here, we have determined the crystal structure of human DSP18 at 2.0 Å resolution. The structure of DSP18 reveals that by adopting a tertiary structure with two antiparallel $\beta$-strands, the CT motif is tightly associated with the catalytic domain; this feature may explain its unusual catalytic activity at high temperature.

## 2. Materials and methods

### 2.1. Expression and purification

DSP18 was cloned from human brain cDNA (Clontech) and subcloned into pET28a. DSP18 (residues 18–188) lacking 17 residues at the N-terminus was expressed in *Escherichia coli* strain BL21(DE3). The deletion of 17 residues was later determined by a trypsin-digestion experiment, which resulted in a DSP18 construct that might produce diffraction-quality crystals. Cells were grown at 291 K after induction with 0.1 m*M* IPTG for 24 h. Cells were harvested and suspended in a lysis buffer containing 50 m*M* Tris–HCl pH 7.5, 500 m*M* NaCl, 1 m*M* PMSF, 0.04%(*v*/*v*) 2-mercaptoethanol, 5%(*v*/*v*) glycerol. After cell lysis by sonication, the His-tagged DSP18 protein was purified by nickel-affinity chromatography. The His tag was removed by trypsin digestion and the protein was further purified by Q-Sepharose ion-exchange chromatography. The catalytic activity of DSP18 (18–188) was checked by monitoring the hydrolysis of 6,8-difluoro-4-methylumbelliferyl phosphate (DiFMUP) using a spectrofluorometric assay. The purified protein was dialyzed against a buffer containing 20 m*M* HEPES–NaOH pH 7.5, 0.2 *M* NaCl, 2 m*M* DTT and 5% glycerol. The protein was concentrated to 10 mg ml$^{-1}$ for use in crystallization.

### 2.2. Crystallization and data collection

Crystallization was performed at 291 K using the hanging-drop vapour-diffusion method. Initial crystallization trials were carried out using commercial screening kits (Hampton Research). The best crystals were grown by mixing 1.8 µl protein (10 mg ml$^{-1}$) solution with an equal volume of reservoir solution containing 0.1 *M* HEPES–NaOH pH 7.5, 10% 2-propanol, 10 m*M* magnesium acetate and 20%(*w*/*v*) PEG 4000 at 291 K. DSP18 crystals grew to their full size after 3 d. X-ray diffraction data were collected at the 4A Macromolecular Crystallography Wiggler Beamline at Pohang Accelerator Laboratory. The crystal in the droplet was transferred to a cryosolution containing the mother liquor supplemented with 20%(*v*/*v*) glycerol for 1 min and flash-frozen in a nitrogen-gas stream at 93 K. The diffraction data were processed and scaled with the programs *DENZO* and *SCALEPACK* from the *HKL*2000 package (Otwinowski & Minor, 1997). DSP18 crystallized in space group $C222_1$, with unit-cell parameters $a$ = 35.74, $b$ = 96.04, $c$ = 116.65 Å, $\alpha = \beta = \gamma = 90^\circ$, and diffracted to 2.0 Å resolution. The crystals tended to show highly anisotropic mosaic splitting along the $b$ axis. Elliptical spot integration in the *HKL*2000 package was judiciously applied to visually minimize spot overlapping in high-resolution bins and the crystal mosaicity was allowed to vary during spot integration, resulting in refined values of between 0.2 and 1.0°. Nonetheless, the severity of mosaic splitting was manifested in relatively high $R_{\rm merge}$ values. The statistics for data collection and refinement are summarized in Table 1.

### 2.3. Structure solution and refinement

The structure of DSP18 was determined by molecular replacement using the VHR structure (PDB code 1vhr) as a search model (Yuvaniyama *et al.*, 1996). The program *EPMR* (Kissinger *et al.*, 1999) placed one catalytic domain of DSP18 in the asymmetric unit of the crystal. Refinement and subsequent model building were carried out using the programs *CNS* (Brünger *et al.*, 1998) and *O* (Jones *et al.*, 1991), respectively. A randomly selected 5% of data were set aside for the $R_{\rm free}$ calculation. Refinement included cycles of simulated-annealing and individual $B$-factor refinement. After these steps, $R$ and $R_{\rm free}$ fell to ∼24 and ∼28%, respectively. At this stage, the electron densities at the C-terminus were apparent

and the remaining residues of the CT motif could be successively built. Strong electron density, not part of the protein, was found near the active-site cavity. We modelled it as a HEPES molecule from the crystallization conditions. Water molecules were gradually added to the model using the waterpick routine in the program *CNS*. The quality of the model was inspected using the program *PROCHECK* (Laskowski *et al.*, 1993). Figures were drawn using the programs *RIBBONS* (Carson, 1997), *GRASP* (Nicholls *et al.*, 1991), *ALSCRIPT* (Barton, 1993), *BOBSCRIPT* (Esnouf, 1997) and *MOLSCRIPT* (Kraulis, 1991).

## 3. Results and discussion

### 3.1. Overall structure

The final model of DSP18, refined at 2.0 Å, comprised 162 amino acids (residues 18–179), one HEPES molecule, one acetate ion and 169 water molecules. In the region from the residue 180 to the C-terminus no clear density is present in the maps and therefore these residues are missing from the model. $R_{\rm cryst}$ and the $R_{\rm free}$ are 15.9 and 18.9%, respectively. The Ramachandran plot, prepared using the program *PROCHECK*, shows that 89.0 and 10.3% of all residues fall within the most favoured and additionally allowed regions, respectively. The catalytic residue Cys104 is in the generously allowed region consistent with well defined electron density. Human DSP18 is a globular protein of approximate dimensions 50 × 30 × 30 Å. The structure of DSP18 can be divided into the catalytic domain (residues 18–159) and the CT motif (residues 160–179) (Fig. 1*a*).

### 3.2. Catalytic domain

The DSP18 catalytic domain (DSP18-C) contains a central twisted five-stranded $\beta$-sheet ($\beta1$–$\beta5$) surrounded by five $\alpha$-helices ($\alpha1$–$\alpha5$). One side of the $\beta$-sheet is covered by one $\alpha$-helix ($\alpha1$) and the other by the remaining four ($\alpha2$–$\alpha5$). In a search for homologous structures using the *DALI* server (Holm & Sander, 1993), several members of the PTP family including VHR (Yuvaniyama *et al.*, 1996), KAP (Stewart *et al.*, 1999) and PTEN (Lee *et al.*, 1999) were identified with similar *Z* values ranging from 13 to 10. VHR is the closest structure and for the structural comparison we superimposed DSP18-C with VHR by using the transformation operator obtained from the *DALI* search (Fig. 1*b*). The transformation operator was further refined with the program *O* using superposition criteria of less than 3 Å deviation for more than three consecutive $C^{\alpha}$ atoms. 136 of 162 $C^{\alpha}$ atoms could be superimposed with a root-mean-square deviation of 1.3 Å.

Although DSP18 aligns well with VHR, substantial differences are also found in several regions. The most prominent difference is the absence of an N-terminal helix and loop, which we refer to as helix $\alpha0$ and loop $\alpha0$–$\beta1$, respectively. Helix $\alpha0$ and the following loop $\alpha0$–$\beta1$ are involved in substrate recognition in VHR and other phosphatases (Yuvaniyama *et al.*, 1996). Deletion of this substrate-recognition motif in DSP18 implies a substrate-recognition mechanism that differs from that of VHR. Other regions that cannot be aligned between DSP18-C and VHR are found in loop $\beta3$–$\beta4$ (Fig. 1*b*). Loop $\beta3$–$\beta4$ is shortened by nine residues in DSP18-C compared with that in VHR. In addition, one helix in VHR which cannot be found in DSP18 is located in

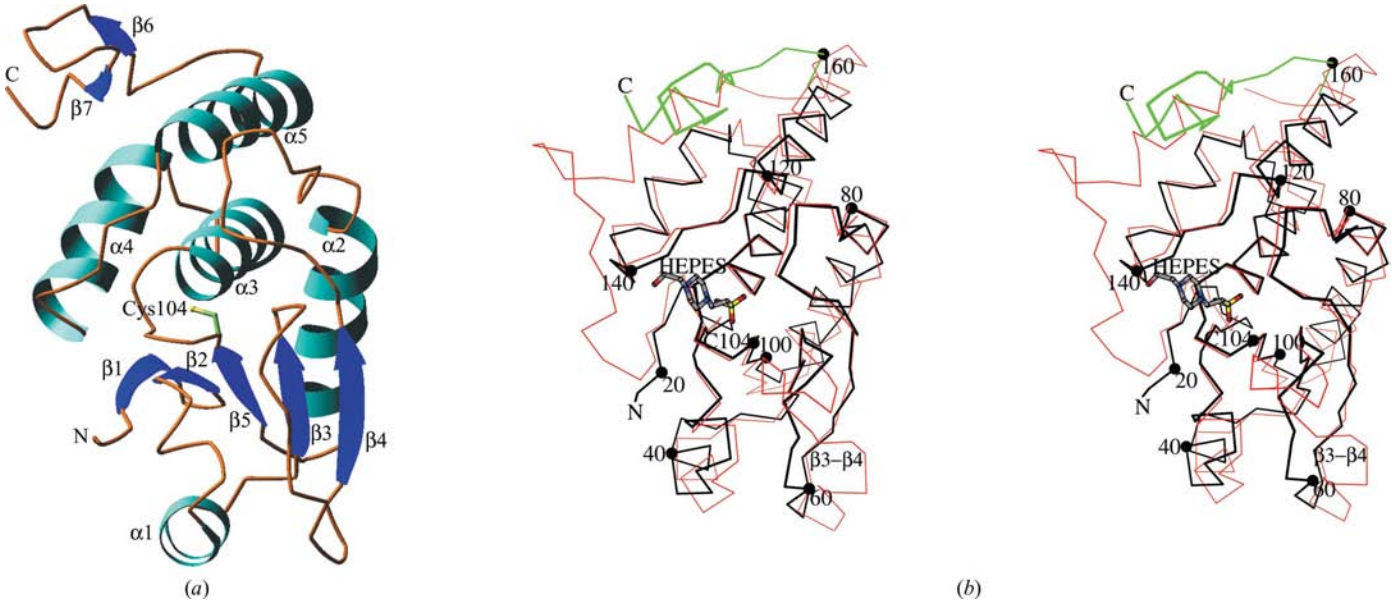


**Figure 1**
Overall structure. (*a*) A ribbon diagram of DSP18. Secondary-structural elements (helices, cyan; strands, blue; loops, orange), which were assigned with the program *PROCHECK*, are labelled. The catalytic cysteine (Cys104) is shown in ball-and-stick representation. The boundaries of the secondary-structural elements are $\beta1$, residues 21–24; $\beta2$, 27–30; $\beta3$, 48–51; $\beta4$, 65–68; $\beta5$, 100–103; $\beta6$, 166–167; $\beta7$, 175–176; $\alpha1$, 38–43; $\alpha2$, 83–95; $\alpha3$, 110–122; $\alpha4$, 127–137; $\alpha5$, 145–159. (*b*) A $C^{\alpha}$ trace of DSP18 is superposed on that of VHR. Every 20th residue of DSP18 is indicated as a black ball and labelled. The catalytic domain and the C-terminal motif of DSP18 are coloured black and green, respectively, whereas VHR is coloured red. The bound HEPES molecule is represented as a ball-and-stick model and the position of the $\beta3$–$\beta4$ loop is indicated.

this loop (Figs. 1*b* and 2). The shorter $\beta3$–$\beta4$ loop in DSP18-C results in a flat active site and in a different hydrogen-bonding network with the residues from the active site (see below).

### 3.3. Active site

The structure near the active site of DSP18-C exhibits the canonical PTP conformation as found in VHR and other PTPs (Yuvaniyama *et al.*, 1996). Alignment of DSP18 and other DSPs reveals that the catalytic triad residues are Asp73, Cys104 and Arg110 (Fig. 2). Cys104 is optimally positioned for nucleophilic attack (Fig. 3*a*). Asp73 in DSP18 also adopts a position similar to that of Asp92 in VHR, which is crucial for PTP activity as a general acid, indicating that Asp73 is likely to function as the general acid in DSP18. Our structural observations are consistent with a previous result in which the D73A mutation resulted in significant activity loss (Wu *et al.*, 2003). However, the hydrogen-bonding interactions with Arg110 in DSP18 are somewhat different from those of the corresponding Arg130 in VHR. In VHR, the side chain of Arg130 interacts with Ala90 from helix $\alpha2$ (Arg130 NH1$\cdots$Ala90 O, 2.9 Å) and with Met69 from loop $\beta3$–$\beta4$ (Arg130 NH2$\cdots$Met69 O, 2.8 Å). The side chain of Arg110 in DSP18 also interacts with a residue from helix $\alpha2$ (Arg110 NH1$\cdots$Val71 O, 2.9 Å) (Fig. 3*a*). In DSP18, however, the residue corresponding to Met69 in VHR is not available for hydrogen bonding as a result of the substantial differences in the $\beta3$–$\beta4$ loop between the two structures (Fig. 1*b* and Fig. 2). Instead, Arg110 makes a bidentate interaction with the side chain of Glu55 from the loop $\beta3$–$\beta4$ (Arg110 NH1$\cdots$Glu55 OE1, 3.0 Å; Arg110 NH2$\cdots$Glu55 OE2, 2.7 Å). The amide atoms of the main chain in the active-site loop and the guanidinium moiety of Arg110 strongly interact with the O atoms of HEPES, which was used as a buffer in crystallization. The interaction distances between the amides of Ala105–Arg110 and the HEPES O atoms are 2.7–3.1 Å. When we superimpose the DSP18 structure on that of VHR complexed with a bisphosphopeptide (PDB code 1j4x), the positions of the sulfate moiety in the DSP18 structure nearly coincide with those of the phosphate group bound at the catalytic site in the VHR structure (Schumacher *et al.*, 2002). Furthermore, the piperazine moiety in HEPES occupies a similar position to that of a phenoxyl group in the structure of the VHR complex. These results suggest that the interaction between DSP18 and HEPES might mimic the catalytic reaction intermediate between a phosphotyrosine (pTyr) substrate and a phosphatase. Therefore, it may provide a platform for the rational design of selective inhibitors to interfere with phosphatase–substrate interactions.

Although the catalytically important residues in DSP18 are align well with those in VHR, the sequence conservation of residues near the active site is quite low. The most prominent differences are found in the P-loop, which spans in the active-site sequence (C)$X_1X_2$G$X_4X_5$(R). The residues in the P-loop of DSP18 (Ala105-Ala106-Gly107-Val108-Ser109) are smaller and have a more hydrophobic character than those of VHR (Arg125-Glu126-Gly127-Tyr128-Gly129) (Fig. 3*b*). The protruding loops $\beta3$–$\beta4$ and $\alpha0$–$\beta1$ in VHR result in a rather deep and narrow active-site pocket, whereas in DSP18 the length of the $\beta3$–$\beta4$ loop is shorter and loop $\alpha0$–$\beta1$ is absent, which results in a flat and wide active-site pocket. In addition to differences in the shape of the active-site pocket, the charge distribution on the DSP18 active-site surface is also quite different from that of VHR (Fig. 3*b*). His70 in loop $\beta3$–$\alpha2$ of DSP18 can be positively charged, while Met69 in the corresponding loop of VHR is neutral. In addition, Ala105 and

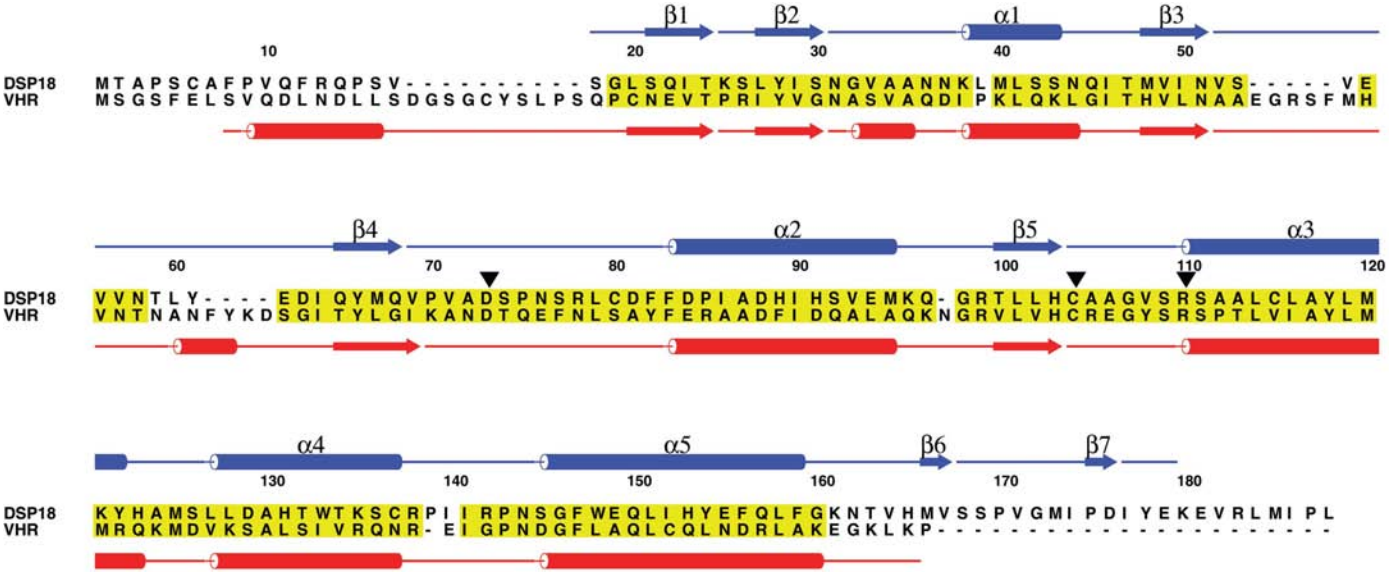


**Figure 2**
Structure-based sequence alignment of DSP18 with VHR. The sequences of DSP18 and VHR were aligned by superposition of the two structures. The superposed residues are shaded yellow in the figure. The secondary-structural elements of DSP18 are shown in blue above the alignment, whereas those of VHR are in red below the alignment. The catalytic triad residues (Asp73, Cys104, Arg110) are indicated as inverted triangles.

Ala106 in DSP18 are neutral, while the corresponding residues Arg125 and Glu126 in VHR are positively and negatively charged, respectively. These results suggest that DSP18 possesses a unique three-dimensional structure and thus might have a distinct specificity profile among DSPs.

### 3.4. Structural implications for the CT motif

The most distinct feature of DSP18 is the existence of a CT motif (residues 160–179; Figs. 1*a* and 1*b*) which is not common to any other known PTPs in terms of amino-acid sequence. The CT motif is found positioned between helices $\alpha$4 and $\alpha$5 of the catalytic domain and is made up of two antiparallel $\beta$-strands ($\beta$6 and $\beta$7). A homologous structure search using the *DALI* server (Holm & Sander, 1993) confirmed that the fold of the CT motif is not found in any other known PTP structures. As shown in Fig. 4(*a*), the catalytic domain and the CT motif interact extensively with each other. The side chains of six residues (Thr163, Val164, Met166, Pro175, Ile177 and Tyr178) in the CT motif are involved in hydrophobic interactions with the catalytic domain. There are also extensive hydrogen-bonding interactions which are mainly localized in the loop region of the CT motif. The side chain of Asn162 from the $\alpha$5–$\beta$6 loop is engaged in hydrogen-bonding interactions with Ile152 and Glu155 (Asn162 ND2···Ile152 O, 2.9 Å; Asn162 ND2···Glu155 OE2, 3.0 Å) and Thr163 makes hydrogen bonds to Leu128 and Glu155 from the catalytic domain (Thr163 OG1···Glu155 OE1, 2.6 Å; Thr163 OG1···Leu128 N, 3.1 Å). The main chain of Met173 from the $\beta$6–$\beta$7 loop is also involved in a hydrogen-bonding interaction with Ser145 (Met173 O···Ser145 OG, 2.7 Å). To confirm whether the conformation of the CT motif is affected by crystal contacts, we examined the neighbouring molecules in the vicinity of the CT motif. There are no serious crystal contacts in the CT motif region of the crystal. The nearest molecule is that generated from a crystallographic twofold axis that runs vertically through the centre between two CT motifs. To analyze these crystal contacts quantitatively, we searched for atoms that make contacts with symmetry-related molecules within a distance of 4 Å. The total number of atoms making crystal contacts is only seven, including one favourable hydrogen-bonding interaction (Ser168 OG···Asp162 OD1 from a symmetry-related molecule, 2.7 Å; Fig. 4*b*). Thus, the conformation of the CT motif observed here is not likely to be affected by crystal packing. The interface between DSP18-C and the CT motif buries 1061 Å$^2$, which corresponds to ∼48% of the total surface area of the CT motif, indicating tight domain–domain associations. DSP18 is known to be active at unusually high temperature (Wu *et al.*, 2003). The tight domain–domain interactions may

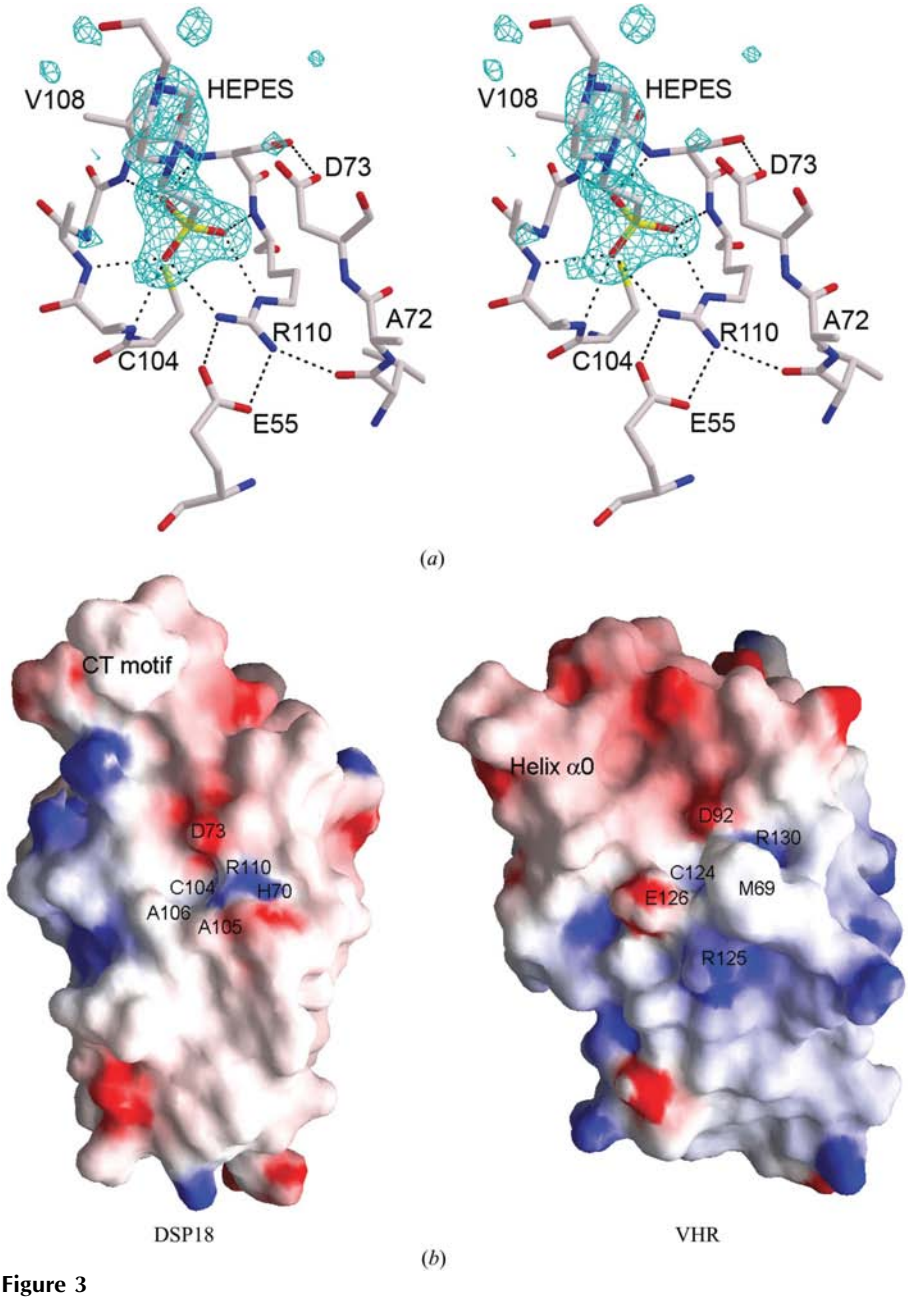


**Figure 3**
Active site. (*a*) The difference electron-density map for DSP18 was generated with the final model, omitting the bound HEPES. The stereo map contoured at the 3.0$\sigma$ level was presented as superposed with the refined model. The hydrogen-bonding interactions around the active site are represented by dashed lines. (*b*) Electrostatic potential surfaces of DSP18 and VHR (PDB code 1vhr) are presented. Positive and negative potentials are coloured blue and red, respectively. Residues near the active site are labelled.

enhance the stabilization of the catalytic domain, which may contribute to the observed thermostability.

## 4. Conclusion

We have presented the first human DSP18 structure at 2.0 Å resolution. Although there is a growing interest in the human PTP family as targets for the development of new drugs (Alonso *et al.*, 2004; Hoffman *et al.*, 2004; Dewang *et al.*, 2005), drug discovery is hampered in part by the difficulties in guaranteeing selectivity owing to the similarity of the PTP active sites. As PTPs are implicated in diverse human diseases, nonspecific inhibitors may result in undesirable signal activation or inactivation. In this respect, elucidation of the structure of DSP18 complexed with HEPES, along with the finding of a unique CT motif, may contribute towards the design of a selective DSP18 inhibitor. In this study, we have also provided a structure-based explanation for the observed thermostability of this enzyme.

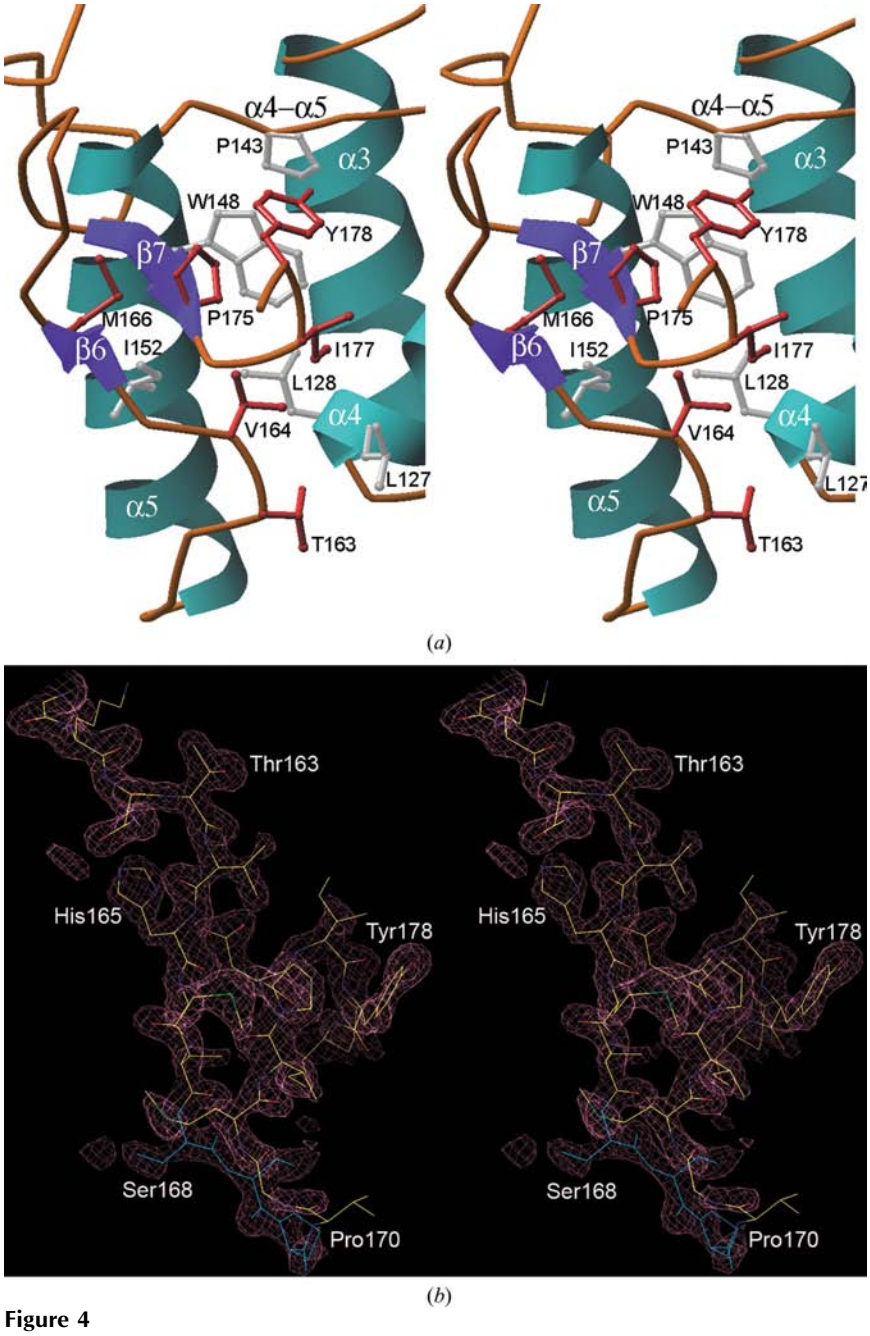


**Figure 4**
CT motif. (*a*) The hydrophobic interactions between the catalytic domain and the CT motif. The side chains of residues involved in the hydrophobic interactions are represented and labelled. Residues in the catalytic domain are coloured grey, whereas those in the CT motif are coloured red. (*b*) Difference $F_o - F_c$ electron-density map around the CT motif omitted for map calculation drawn in stereo with the refined model. The map was contoured at a level of 3.0$\sigma$. Residues with atoms that participate in crystal contacts with neighbours are coloured cyan.

We would like to thank Dr H. S. Lee and the staff of Pohang Accelerator Laboratory 4A Macromolecular Crystallography Wiggler Beamline for their help with data collection. This research was supported by a grant from the KRIBB Research Initiative Program.

## References

Alonso, A., Sasin, J., Bottini, N., Friedberg, I., Friedberg, I., Osterman, A., Godzik, A., Hunter, T., Dixon, J. & Mustelin, T. (2004). *Cell*, **117**, 699–711.
Alonso, A., Saxena, M., Williams, S. & Mustelin, T. (2001). *J. Biol. Chem.* **276**, 4766–4771.
Barton, G. J. (1993). *Protein Eng.* **6**, 37–40.
Brünger, A. T., Adams, P. D., Clore, G. M., DeLano, W. L., Gros, P., Grosse-Kunstleve, R. W., Jiang, J.-S., Kuszewski, J., Nilges, M., Pannu, N. S., Read, R. J., Rice, L. M., Simonson, T. & Warren, G. L. (1998). *Acta Cryst.* D**54**, 905–921.
Camps, M., Nichols, A. & Arkinstall, S. (2000). *FASEB J.* **14**, 6–16.
Carson, M. (1997). *Methods Enzymol.* **277**, 493–502.
Chang, L. & Karin, M. (2001). *Nature (London)*, **410**, 37–40.
Dewang, P. M., Hsu, N., Peng, S. & Li, W. (2005). *Curr. Med. Chem.* **12**, 1–22.
Esnouf, R. M. (1997). *J. Mol. Graph.* **15**, 112–134.
Farooq, A. & Zhou, M. M. (2004). *Cell. Signal.* **16**, 769–779.
Hoffman, B. T., Nelson, M. R., Burdick, K. & Baxter, S. M. (2004). *Curr. Pharm. Des.* **10**, 1161–1181.
Holm, L. & Sander, C. (1993). *J. Mol. Biol.* **233**, 123–138.
Jones, T. A., Zou, J.-Y., Cowan, S. W. & Kjeldgaard, M. (1991). *Acta Cryst.* A**47**, 110–119.
Kissinger, C. R., Gehlhaar, D. K. & Fogel, D. B. (1999). *Acta Cryst.* D**55**, 484–491.
Kraulis, P. (1991). *J. Appl. Cryst.* **24**, 946–950.
Laskowski, R. A., MacArthur, M. W., Moss, D. S. & Thornton, J. M. (1993). *J. Appl. Cryst.* **26**, 283–291.
Lee, J. O., Yang, H., Georgescu, M. M., Di Cristofano, A., Maehama, T., Shi, Y., Dixon,

J. E., Pandolfi, P. & Pavletich, N. P. (1999). *Cell*, **99**, 323–334.
Nicholls, A., Sharp, K. A. & Honig, B. (1991). *Proteins*, **11**, 281–296.
Otwinowski, Z. & Minor, W. (1997). *Methods Enzymol.* **276**, 307–326.
Schumacher, M. A., Todd, J. L., Rice, A. E., Tanner, K. G. & Denu, J. M. (2002). *Biochemistry*, **41**, 3009–3017.
Stewart, A. E., Dowd, S., Keyse, S. M. & McDonald, N. Q. (1999). *Nature Struct. Biol.* **6**, 174–181.
Wu, Q., Gu, S., Dai, J., Dai, J., Wang, L., Li, Y., Zeng, L., Xu, J., Ye, X., Zhao, W., Ji, C., Xie, Y. & Mao, Y. (2003). *Biochim. Biophys. Acta*, **1625**, 296–304.
Yuvaniyama, J., Denu, J. M., Dixon, J. E. & Saper, M. A. (1996). *Science*, **272**, 1328–1331.